FUTURE TRENDS IN PREDICTING THE COMPLEX FRACTURE BEHAVIOUR OF RUBBER MATERIALS

Radek Stoček*[1], Martin Stěnička[1], Petr Zádrapa[1]

[1]Centre of Polymer Systems, Tomas Bata University in Zlín, Tomas Bata Av. 5678, Zlín, Czech Republic

*Corresponding author (e-mail: stocek@utb.cz, tel: +420 57 603 8010)

ABSTRACT

Future trends in predicting the fracture behaviour of rubber materials (products) are discussed. A complex methodology for the determination of rubber fracture behaviour from the energy viewpoint based on simulating realistic loading conditions in services applied to a rubber matrix in a laboratory test set-up is introduced. Because this is a pure rubber matrix investigation, additional effects such as rubber product design or assembling the final performance can be fully avoided. This methodology requires instrumented and automated laboratory equipment – an Intrinsic Strength Analyser (ISA) and a Tear and Fatigue Analyser (TFA) which represent the first commercialization of a classic method for assessing long-term durability. These testing methods are applied to quantify the behaviour of rubber compounds over a broad range of tearing energies – from the fatigue threshold up to the critical tearing energy or the ultimate tear strength T_C to determine the relationship between fatigue crack growth (FCG) rates d*a*/d*n* *vs.* the tearing energy *T*. This complex methodology was evaluated for carbon black (CB) reinforced compounds based on pure natural rubber (NR) and butadiene rubber (BR) typical for tire applications. Finally, the determined data were correlated with previous work done by Lake and Lindley (1965) as well as with practical experiences of tire manufacturers.

Keywords: Rubber, Fracture, Fatigue, Crack, Tearing, Energy

1. INTRODUCTION

It is a well-known fact that rubbers are visco-elastic materials. Owing to their visco-elastic nature, compared to other engineering materials like metals, products made from rubbers exhibit time-dependent behaviour. This means that the capability of a rubber product to perform under a given set of loading conditions worsen during service. Therefore, it is highly important to predict how long a rubber component can effectively perform in the environmental surrounding in which it is placed to do the work. In this contest, rubber products manufacturers and raw materials suppliers are actively seeking reliable and accurate laboratory testing methodologies to estimate the performance of rubber products during their service. Ideally, predictive laboratory tests should balance accuracy, relevance, and reproducibility. They should connect fundamental principles which show how results from a simple sheet of cured rubber are related to realistic loading conditions during service. The rapid advancement of simulation technology is one of the ways to do so. Simulation technology has created a new opportunity to link

material laboratory testing to the real-rubber product performance during service. In order to generate knowledge about the complex fracture behaviour of the rubber matrix, comprehensive experimental investigations are necessary, which is one key point of this work. Finally, characterizing complex fracture behaviour for simulating realistic loading conditions in service applied to a pure rubber matrix in a laboratory test set-up promises to gain complex information about the material in an early stage of development before rubber products have been produced or even before designs are finalized. Furthermore, such an approach would enable quicker development times and minimize extensive real rubber product tests before production.

Generally, the fracture of materials is mostly an undesirable process that reduces the service life of its structural components dramatically. Defects and flaws are very common in every real material and act as initiators of macroscopic cracks. Due to the complex design and composition of different products, the fracture mechanics need to focus on investigating cracks in samples having specific geometry. As mentioned above, owing to their visco-elastic nature, rubbers exhibit large deformations even under small external forces above their glass transition temperature. Therefore, rubber materials are reinforced with hard nanostructured fillers to enhance different mechanical properties such as strength, hardness, stiffness, abrasion resistance, reduction of heat build-up or crack growth resistance. The resulting multi-scale structural hierarchies influence the fracture mechanical behaviour of the rubber due to the phase morphology, the distribution and the dispersion of fillers and the multi-scale structure of the fillers themselves.

The strength of rubbers depends on their chemical structure, as well as on their visco-elastic behaviour near crack tip [1, 2]. Due to visco-elastic energy dissipation, the total energy required to propagate a crack in rubbers is significantly greater than the energy associated with the intrinsic strength of the molecular structure. Traditional testing methods used in the rubber industry to measure tear and crack growth properties are not effective to perform detailed structure-property relationship studies that are necessary for a rational design of improved compounds for demanding applications such as tires, seals, belts, bashing elements, and other rubber products. Assigning a clear responsibility for crack growth resistance to the structural features of compounds is very difficult because the same material characteristics influence the hysteresis behaviour of the rubbers, which is a very large contributor to the bulk fracture response that is measured.

If a crack grows in a cross-linked polymer, the polymer chains crossing the plane of the crack rupture. Fig. 1 shows a schematic visualization of the rupture of a polymer chain. It is clear that due to the applied deformation, the chains are strained in the direction of the principal strain. When the strain energy exceeds the value of the intrinsic strength, the chains rupture and a crack propagates orthogonally to the principal strain with respect to the polymer chains. Thus, all chains behind the crack tip are ruptured and all chains in front of the crack tip are strained, whereas the strain decreases with increasing distance from the crack tip. Finally, the dissipation field in the vicinity of the crack tip field is clearly associated with the strain of the chains.

However, the dissipation, the respective stress and the strain fields near the crack tip are unknown neither quantitatively nor qualitatively. Thus, characterizing local fields near the crack tip, as in the case of brittle materials, is not accurate. Therefore, the global energy balance in a sample undergoing crack growth as a generalization of Griffith's approach [3] seems to be the sole candidate for characterizing a fracture in such materials [4].

Considering the process of incremental crack propagation in a solid, the global energy balance under quasi-static conditions equation 1:

$$\frac{dW_{ext}}{dA} - \frac{dW}{dA} = \frac{dW_{sep}}{dA} + \frac{dW_{dis}}{dA} \tag{1}$$

where W_{ext} is the external work, W is the recoverable elastic strain energy, W_{dis} is the dissipated energy and W_{sep} is the local work of separation. In the case of a plane sample with a constant thickness, B and a straight crack tip, the increment of a crack area is dA = B da, where da denotes the crack length increment. The left-hand side of equation 1 is called the energy release rate [3], which is the energy released during crack propagation. The right-hand side is the energy dissipation rate [3, 5–8] also labelled as the tearing energy T [4] in the case of rubber materials. It could be understood as the energy needed to advance a fracture plane by one unit area including all energy losses due to accompanying dissipative processes.

Considering that the external work is zero, *i.e.* the clamp distance l is constant during the process of crack propagation, the original proposition made by Rivlin and Thomas [4] for the determination of tearing energy T can be derived:

$$T = -\left.\frac{dW}{dA}\right|_{l=const.} = -\left.\frac{dW}{B\,da}\right|_{l=const.} \tag{2}$$

Because of their viscoelastic behaviour, the rubber components, when exposed to dynamic and cyclic loading conditions, lead to fatigue. This assumption needs to be taken into account to understand the influence of the loading conditions of the rubber product in service and to apply the corresponding conditions in the laboratory test. Therefore, in [9, 10] the FCG rate da/dn in dependence on the energy release rate or tearing energy T has been experimentally determined for different rubber materials. Fig. 2 shows a typical relationship for a rubber material in a double-logarithmic plot. Lake and Lindley [10] firstly described various regions in this plot characterizing different tearing behaviours. The FCG rate da/dn depends on the tearing energy T in each of the relevant regions in a characteristic manner. In the first region, there is a minimum energy requirement for the fracture process. For unfilled rubber, this minimum energy depends primarily on the details of the polymer network, such as the average molecular weight between the cross-links, and the weakest bond in the main polymer chain [11]. It is largely independent on time, temperature and the degree of swelling. Therefore, it is often called intrinsic strength T_0 [12]. As long as the value of the tearing energy T is lower than T_0, FCG proceeds at a constant rate and it is independent of the dynamic loading, but affected by the environmental attack. The stable crack growth region is followed by the transient state, which occurs immediately after the region of the intrinsic strength. The region of stable crack growth is between the values of the tearing energies T_1 and T_2. This region is described with the relationship between the FCG rate da/dn and tearing energy T by the power law proposed by Paris and Erdogan [13]:

$$T_1 \le T \le T_2 \rightarrow \frac{da}{dn} = \beta\,\Delta T^m \tag{3}$$

where β and m are material constants. The FCG rate da/dn, and the tearing energy T can be approximated by the formula in the following range:

$$10^{-9}\ \frac{mm}{cycle} < \frac{da}{dn} \leq 10\ \frac{mm}{cycle}\ and\ T \approx 50\ \frac{J}{m^2} + 5{,}000\ \frac{J}{m^2} \tag{4}$$

Finally, the crack proceeds to the unstable fatigue growth and the FCG rate become essentially infinite.

The endurance limit respective intrinsic strength T_0 marks the lower limit of the FCG rate curve as shown in Fig. 2. [5, 14] A crack operating at an energy release rate below the intrinsic strength can be projected to operate indefinitely without growing, since there is simply not enough energy supplied to break polymer chains at the crack tip. [15, 16] Therefore, this endurance limit T_0 or mechanical fatigue limit is very useful in product design and in fatigue analysis. [17]. Knowing the value of the intrinsic strength of rubber components in the process of compound development, the service life depending on the real loading conditions can be predicted. Furthermore, suitable rubber materials could be chosen based on their intrinsic strength data to enhance the service life of the product. It can be stated that materials with a high intrinsic strength value are resistant to fracture processes, which occur at a low level of tearing energy *T*. Only a few scientific publications have been elaborated in terms of defining a methodology for the evaluation of the intrinsic strength. However, the pioneering work by Lake and Yeoh [18] based on cutting methods experimentally associated the intrinsic strength with the intrinsic cutting energy $S_{0,C}$. Based on this theory, the main effort in elaborating the theoretical background was done by Mars [17]. The complete methodology described by Lake and Yeoh [18] was redefined and reworked by Mars into the current state-of-the-art and patented in 2017 [19]. From the equipment point of view, there was an instrument missing which would be able to determine the intrinsic strength quantitatively. Stocek *et al.* [20] introduced a prototype of laboratory equipment which was able to characterize the intrinsic strength based on a precisely defined cutting procedure. Finally, as described in [15], the fully instrumented equipment labelled ISA (Co. Coesfeld GmbH, Germany) inclusively the implemented cutting procedure based on the Lake and Yeoh methodology [18] has industrially been introduced and validated.

In terms of the stable crack growth region, a very important reason to determine the resistance of rubber against FCG is that defects and flaws exist in all real rubber products and they act as initiators of macroscopic cracks. From the theory, it is well-known that there is an increased energy dissipation due to geometrical irregularities. With increases in the irregularity or decreases in the edged shape, the energy dissipation increases exponentially. Many experiments describing the FCG of various rubber types and different compositions, a broad range of loading conditions, the influence of fillers, curing agents, anti-oxidants and environmental conditions (temperature, ageing) have been performed all over the world [9, 14, 21–25]. The main scientific works are concentrated on investigating the FCG in the tensile mode as discussed previously, whereas Rivlin and Thomas [4] have undertaken the pioneering work in this research field. There are a few types of testing facilities, investigating the fatigue fracture of rubber materials in the world, *e.g*. fatigue to failure tester, DeMattia, Flexometer, or various dynamic tensile analysers. The only testing facility worldwide which is based on quantitative analyses of FCG with in-situ automated measurement of crack growth is the Tear and Fatigue Analyser **(**TFA) produced by Co. Coesfeld GmbH, Germany. A detailed description of the testing facility is presented elsewhere [26–28].

Finally, the value of the ultimate strength T_C marks the highest limit of the FCG rate curve, which is illustrated in Fig. 2. Beyond this value, the total rupture of rubber proceeds without any additional energy input. Due to the instrumental difficulties encountered for a solution for a large deformation finite elasticity problem, Rivlin and Thomas [4] performed a systematic experimental investigation, in which the ultimate strength or critical tearing

energy T_C have been determined in terms of applied forces and displacements. They were able to calculate the critical tearing energy T_C for different rubber materials. Many scientists have demonstrated (cf. [29–31]) that the critical tearing energy T_C does not depend on the geometry of the sample, but it is considered to be a material property. From the experimental point of view, fundamental work for determining the critical tearing energy T_C describing the unstable crack growth, has been done by Gent and Henry [32] by using constrained trousers specimen. However, this type of specimen is applicable only for quasi-static tensile loading. In the past, many researchers investigated the value of critical tearing energy T_C with respect to various rubber types and compositions. However, most of these publications were again focused on quasi-static or dynamic impact loading conditions by using the uniaxial tensile specimen [33–35]. Moreover, there are no records available in the literature regarding the experimental investigations of the critical tearing energy T_C causing the unstable crack growth under fatigue loading conditions. The main difficulties for the experimental estimation of the ultimate strength T_C under fatigue loading conditions can be seen in a highly accelerated fracture process when reaching the critical value compared to significantly slower processes below this value. Thus, there are very high demands on technical solutions for the experimental FCG investigation in a broad range of tearing energies. Experimentally, the ultimate strength T_C can be determined with both previously mentioned equipment, namely ISA and TFA. The TFA determines the critical tearing energy T_C under the application of fatigue loading conditions, whereas ISA under the quasi-static loading condition only.

Finally, the main question is: How can the knowledge of complex fracture behaviour over a broad range of tearing energies (from the endurance limit T_0 up to the ultimate strength T_C) be beneficial for predicting the lifetime of rubber products? If the FCG of rubber is known in the complete range of applicable tearing energies, the product can be applied to a broader range of tearing energies and thus it can be efficiently used over its complete applicability or durability, respectively. Therefore, the applicability of the rubber product would be rapidly enhanced and the product would have a reasonable higher benefit. In conclusion, it is necessary to estimate the complete Paris-Erdogan plot in the range from the fatigue threshold, respective endurance limit T_0, up to the ultimate strength T_C for the complex description of the fracture behaviour of pure rubber matrix material with respect to the final product application, respective loading conditions.

For these reasons, the main aims of this article are firstly to introduce a complex methodology for estimating the complete Paris-Erdogan plot from the endurance limit T_0 up to the ultimate strength T_C, and secondly validating this methodology by using rubber materials, whose fracture behaviour is well-known from both, practical and scientific point of view.

2. EXPERIMENTAL

The material used in this work are natural rubber (NR, SMR 20 CV/BP1, Lee Rubber Co. Pte Ltd., Malaysia) and butadiene rubber (High-Cis Nd-BR, Trinseo, Germany) filled with 50 phr of CB N339. Table 1 lists the formulations of the compounds used based on these rubbers.

A two-step mixing procedure was employed to prepare all rubber compounds. Both steps were undertaken with an internal mixer SYD-2L (Everplast, Taiwan) at a rotor speed of 50 rpm and a temperature of 100 °C with a fill factor of 0.7. First, the masterbatch was prepared after masticating the virgin rubber for 1 min. To this, carbon

black was added and it then mixed for further 5 min. The masterbatch prepared was milled using a double-roll mill and sheeted out at a temperature of 60 °C. The final batch was then prepared by mixing the masterbatch for 1 min at a rotor speed of 35 rpm and at a temperature of 60 °C followed by adding the complete curing system and mixed for 5 min. The final batch was milled again using a double-roll mill at 60 °C. After storing for 24 hrs, the curing properties were determined by moving die rheometer MDR 3000 Basic (MonTech, Germany) according to ASTM 6204 at a temperature of 160 °C.

The specimens having different geometries were cured in a heat press LaBEcon 300 (Fontijne Presses, The Netherland) at a temperature of 160 °C under the estimated optimum curing time t_{90}+1 min per 1 mm of thickness. The pure-shear specimens having dimensions of L_0=10 mm, W_P=100 mm, and B=1.5 mm for ISA, and L_0=4.0 mm, W_P=40 mm, and B=1.0 mm for FCG analyses are shown in Fig. 3. Standard sheets (150 mm×150 mm×2 mm) were cured for the determination of fundamental tensile properties. Finally, specimens having a thickness of 6 mm were also cured for hardness and abrasion testing.

The tensile properties, Shore-A hardness and abrasion resistance, were measured. The tensile test was performed at an extension rate of 500 mm/min for rectangular test specimens (80 mm×10 mm×2 mm) with the initial distance between clamps of 30 mm. The tensile properties reported in this study are an average of 10 specimens. The measurement of the Shore-A hardness was performed as described in the industrial standard ISO 7619-1. The reported results are the medians of 5 samples for each compound. The determination of abrasion resistance for 3 replicate samples for each compound was performed as defined in the industrial standard ISO 4649 B, this method is based on determination of the abrasion volume loss ΔV_{rel} due to the abrasive action of sliding a test piece over 40 m length of a specified grade of abrasive sheet.

The endurance limits T_0 and the intrinsic strength have been analysed by using the ISA (Fig. 4) which was operated by following the testing methodology, developed by Endurica (LLC, USA) [19].

A schematic representation of the measuring principle is shown in Fig. 5. A specimen of pure-shear geometry (Fig. 3), which is pre-cracked on one edge, is exposed to several different strain levels in a range from 0 to 0.5. The specimen is held under each defined strain and allowed to equilibrate for 10 min. Afterwards, the stress is determined from the normal force before cutting. The stress-strain curve is generated by combining the results from the different strain levels. When equilibration is reached (at each given strain), a highly sharpened blade (length×width×thickness: 43 mm×22.2 mm×0.10 mm) is brought into contact with the crack tip and it is driven to slice the specimen at three constant sequential rates, that are decreasing in value (from 10 mm/min to 0.1 mm/min to 0.01 mm/min). The steady state reaction force on the blade during cutting F is measured at each cutting rate for each strain level.

For the pure-shear specimen under strain without the blade, the tearing energy T is computed as the product of the strain energy density W and the unstrained section gauge height L_0:

$$T = W\, L_0 \tag{5}$$

The strain energy density W in the specimen is determined as a function of the strain by numerically integrating the stress-strain curve.

While cutting with the blade, the moving force *f* required to maintain a constant rate of cutting imparts an additional contribution to the total energy release rate, driving the crack tip. It is called the cutting energy F_C and its value is given by equation 6:

$$F_C = \frac{f}{B} \tag{6}$$

where *B* is the thickness of the specimen.

When crack tip dissipation is sufficiently small, the intrinsic cutting energy $S_{0,C}$ for strained pure-shear specimen, undergoing the cutting process, may be written as the sum of the tearing energy *T* and the cutting energy F_C:

$$S_{0,C} = T + F_C \,. \tag{7}$$

The intrinsic cutting energy $S_{0,C}$ is determined via the measurements. It was measured on 3 samples for each compound.

The intrinsic strength T_0 (endurance limit) is proportional to the intrinsic cutting energy $S_{0,C}$ with a proportionality constant *b* which is a function of the blade sharpness:

$$T_0 = b\, S_{0,C} \tag{8}$$

The proportionality constant *b* can be obtained by testing the calibrated material in the ISA, whereas according to Lake and Yeoh [18] an unfilled styrene-butadiene-rubber (SBR) was used, for which the value of the intrinsic strength T_0=60 J/m^2 (endurance limit) is known. An unfilled emulsion-SBR (E-SBR 1500, Trinseo, Germany) was used as the reference (SBR_{ref}) rubber in combination with other chemical ingredients listed in Table 2. The SBR compound has been mixed and cured in same manner as the NR and BR compounds.

A schematic example of the way to assess $S_{0,c}$ from data, collected using the ISA, is given in Fig. 6. A line with a slope of -1 on the cutting energy F_C *vs.* the tearing energy *T* plot (corresponding to equation 7) which intersects with the data curve at the lowest possible point, allows for quantifying the intrinsic cutting energy $S_{0,c}$ as the intercepts of the line with the graph axes.

The stable crack growth as well as the ultimate strength T_C have been determined with the TFA shown in Fig. 7 (left) and a detailed view of the isolated testing chamber is visible in Fig. 7 (right). Since the machine is equipped with three independent electric dynamic drives, three different loading conditions of rubber materials can be analysed simultaneously, whereas three double-notched mini pure-shear (mPS) samples are investigated at each dynamic drive. The crack growths of each rubber test specimen can be monitored through an image process system with a CCD camera, which moves from one specimen to the next and captures a photo of the concerned sample. Simultaneously, the picture is digitalized and the software localizes in-situ the crack position, determines the contour length and calculates the contour length increment.

To achieve a highly reproducible measuring process, it is necessary to work quantitatively and to use a very clearly defined methodology. Thus, the following testing methodology has been developed to obtain reliable data with good quality:

I. Determining tearing energy *T*

a) Sample fixing

b) Pre-conditioning

c) Tearing energy *T* determination

d) Tearing energy *T* evaluation

II. Notching the initial crack

III. Crack growth measurement setting for the optical measuring system

IV. FCG analyses

V. Evaluating the crack growth rate d*a*/d*n* dependent on the tearing energy *T*

In Table 3, the boundary conditions used for the complete FCG analyses are listed. In the first step, the tearing energy has been determined as a function of displacement for a set of four varied strains 0.1, 0.3, 0.5 and 0.7. In the next step the quadratic fitting function has been evaluated for each compound.

The tearing energies *T* have been evaluated from the determined data sets in line with equation 4. Finally, the applied strains for the FCG analyses have been calculated from the quadratic fitting functions, given for required tearing energies *T* from 150 up to 3,000 J/m^2.

3. RESULTS

Table 4 represents the mechanical properties of the compounds determined from the standard tensile testing method. The values of the stress at 300 % elongation are similar for both materials. This comparably large stiffness under large strain is expected due to the concentrations of sulphur cross-linker and the CB filler being held constant throughout the formulations. However, there were some differences in the low strain stiffness data. For instance, the stress at 100 % elongation and Shore-A hardness are listed in Table 5. This is presumably due to differences in the filler networking / micro-dispersion within the different polymer matrices. The abrasion resistance inversely followed the Shore-A hardness with less volume loss (higher abrasion resistance) corresponding to a higher Shore-A hardness (Table 5). The relative ranking of the abrasion resistance, which is large for BR than for matches the knowledge concerning the polymer type dependence. It means that the variations in abrasion volume loss cannot be solely attributed to the compound hardness.

The relationship between the cutting energy F_C and the tearing energy *T* for both analysed compounds, the intrinsic cutting energy $S_{0,C}$ values are determined and plotted in Fig. 8. The intrinsic cutting energies $S_{0,C}$ are determined and associated in the plot to each function and rubber type.

The simplicity of the formulas in a complex nature of the various compounds makes it simple to rationalize the observed dependence of intrinsic cutting energy $S_{0,C}$ on the type of rubber used. In the case of the analyzed rubbers, a lower intrinsic cutting energy $S_{0,C}$=482.07 J/m^2 was found for the compound based on NR, which is caused by its strain crystallizing nature causing the lower cutting forces over an applied range of tearing energies. The higher intrinsic cutting energy $S_{0,C}$=949.23 J/m^2 exhibits the compound based on BR. The force-time traces, where a higher cutting force was determined for the non-strain crystallizing BR at a lower tearing energy level *T* points out a higher elasticity of this material which is the reason for the higher intrinsic cutting energy of BR.

From the plot of the cutting energy F_C *vs.* the tearing energy T as shown in Fig. 9, the intrinsic cutting energy $S_{0,C}$=571.61 J/m^2 was determined for the reference rubber material. From the intrinsic cutting energy $S_{0,C}$ and the above given intrinsic strength T_0 for the reference rubber material, the proportionality constant b was evaluated using equation 8 and thus the applied blade can be calibrated. The proportionality constant b was determined as 0.105. Using this calibrating constant, the intrinsic strength T_0 for both analysed materials was calculated and the values are listed in Table 6.

It is widely known in the tire industry that BR compounds have significantly greater wear resistance than NR compounds in tire treads. We were able to confirm this trend via DIN abrasion testing, which gave losses of 175 mm^3 for NR and 52 mm^3 for BR. The very significant fatigue threshold difference for the two materials (T_0=50.62 J/m^2 for NR and T_0=99.67 J/m^2 for BR) seems to be connected with their disparate wear behaviour. There is a distribution of tearing energies coming from a distribution of sliding impacts imposed on a tire tread surface from diverse road micro-asperities. Any of these events that result in a tearing energy below T_0 does not contribute to damage accrual and related wear. This testing method quantifies the fatigue threshold of a rubber compound in a few hours, which is an amazing contribution to fasten the development of long-term durable rubber products. Whereas, previous methods required weeks or months to determine the near-threshold data. The values of the experimentally determined tearing energies from the FCG analyses in relation to the strain-based analyses of 3 samples for both rubbers are plotted in Fig. 10. The average values are fitted with quadratic polynomials and the equations of these functions are listed.

The type of rubber, depending on the FCG rate of the analysed compounds, is shown in Fig. 11. It shows the values of the Paris-Erdogan equation determining the dependence to the FCG rate, da/dn on the tearing energy T in Table 7. The material parameter m defining the slope of the ability of the crack to propagate, clearly points out that NR is the more resistant rubber to the FCG due to its strain induced crystallinity, which causes the improved resistance to FCG with increasing the tearing energy T. The higher slope of the material parameter m for BR indicates that this material generally has a lower resistance to the FCG with an increasing tearing energy T. The curve of the FCG rate da/dn as the function of the tearing energy T of BR crosses the curves for NR approximately at the tearing energy T=300 J/m^2. Thus, BR is more resistant to FCG below this given energy compared to NR. This observation corresponds with the previously determined data from Lake and Lindley. [10].

Contrasting the abrasion volume loss data with the FCG results for the compounds in Fig. 10, it is clear that abrasion resistance is not simply related to crack growth resistance. They have exactly opposite trends for both of the CB reinforced compounds.

The critical tearing energy T_C plotted in the Fig. 12 was determined as the tearing energy T associated with the strain ε where the crack grows without any other energy input. A higher critical tearing energy T_C=18,485 J/m^2 exhibits the compound based on NR, whereas a lower critical tearing energy T_C=3,265 J/m^2 was determined for BR compound.

Finally, the reconstructed complete relationships for the FCG rate da/dn as a function of the tearing energy T for both analysed compounds containing all phases of the fracture processes are plotted in Fig. 13. The relationship of the FCG rate da/dn *vs.* the tearing energy T can be determined from the endurance limit T_0 up to the ultimate strength T_C in a very fast way within few hours.

4. CONCLUSIONS

In this work, future trends in predicting the fracture behaviour of rubber materials, respective products made from them, were introduced. A complex methodology to determine the fracture behaviour from an energetic point of view was applied and discussed. To this end, the simulation of realistic loading conditions in service is applied in laboratory tests to the pure rubber matrix. The carbon black reinforced compounds based on pure NR and BR have been investigated using two testing methods, namely the ISA and FCG analyses, to quantify the compounds over a broad range of tearing energy levels, from the fatigue threshold up to the critical tearing energy. Thus, the complex fracture behaviour described in relation to the FCG rate da/dn *vs.* the tearing energy T was firstly quantitatively determined from the endurance limit T_0 up to the ultimate strength T_C in a very fast way within few hours. The determined data for the experimental analysis of the rubber materials, used in this work, clearly corresponds with the previously evaluated data from the work undertaken by Lake and Lindley (1965). Thus, receiving identical data over the broad range of tearing energies by using the introduced complex methodology demonstrates a huge potential and efficiency improvement. Characterizing complex fracture behaviour with respect to realistic loading conditions in a laboratory test set-up promises to gain complex information about the material in the early stages of development before rubber products have been produced or even before designs are finalized. This approach promises to optimize rubber products in terms of performance and durability. Furthermore, it enables quicker development times and minimizes extensive real rubber product tests before production.

ACKNOWLEDGEMENT

This article was written with the support of the project Centre of Polymer Systems – Strengthening Research Capacity (reg. number: CZ.1.05/2.1.00/19.0409) as well as NPU I (LO1504).

REFERENCES

[1] Lake, G.J., Yeoh, O.H.: Effect of crack tip sharpness on the strength of vulcanized rubbers. J. Polym. Sci., Part B: Polym. Phys. 25, 1157–1190 (1987)

[2] Bhowmick, A.K.: Threshold fracture of elastomers. J. Macromol. Sci., Polym. Rev. 28, 339–370 (1988)

[3] Griffith, A.A.: The phenomena of rupture and flow in solids. Philos. Trans. R. Soc. London, Ser. A 163–198 (1921)

[4] Rivlin, R.S., Thomas, A.G.: Rupture of rubber. I. Characteristic energy for tearing. J. Polym. Sci. 10, 291–318 (1953)

[5] Andrews, E.H.: Rupture propagation in hysteresial materials: Stress at a notch. J. Mech. Phys. Solids 11, 231–242 (1963)

[6] Sumpter, J.D.G.: An alternative view of R curve testing. Eng. Fract. Mech. 64, 161–176 (1999)

[7] Sumpter, J.D.G.: The energy dissipation rate approach to tearing instability. Eng. Fract. Mech. 71, 17–37 (2004)

[8] Persson, B., Albohr, O., Tartaglino, U., *et al.*: On the nature of surface roughness with application to contact mechanics, sealing, rubber friction and adhesion. J. Phys.: Condens. Matter 17, R1–R62 (2005)

[9] Gent, A.N., Lindley, P.B., Thomas, A.G.: Cut growth and fatigue of rubbers. I. The relationship between cut growth and fatigue. J. Appl. Polym. Sci. 8, 455–466 (1964)

[10] Lake, G.J., Lindley, P.B.: The mechanical fatigue limit for rubber. J. Appl. Polym. Sci. 9, 1233–1251 (1965)

[11] Lake, G.J., Thomas, A.G.: The strength of highly elastic materials. Proc. R. Soc. London, Ser. A 300, 108–119 (1967)

[12] Gent, A.N., Mars, W.V.: Strength of elastomers. In: Mark, J., *et al.*: (eds.) Science and Technology of Rubber, 4th Edition, Chapter 10, pp. 473–516. Academic Press (2013)

[13] Paris, P., Erdogan, F.: A critical analysis of crack propagation laws. *J. Basic Eng*. 528–534 (1963)

[14] Lake, G.J., Lindley, P.B.: Mechanical fatigue limit for rubber. Rubber Chem. Technol. 39, 348–364 (1966)

[15] Mars, W.V., Kipscholl, C., Stocek, R.: Intrinsic Strength Analyser based on the cutting method. In: Proc. of the Fall 190th Technical Meeting of the Rubber Division of the American Chemical Society. Pittsburgh, USA, 10–13 (2016)

[16] Robertson, C.G., Stocek, R., Kipscholl, C., *et al.*: Characterizing the intrinsic strength (fatigue threshold) of natural rubber/butadiene rubber blends. Tire Sci. Technol. 47, 292–307 (2019)

[17] Mars, W.V.: Fatigue life prediction for elastomeric structures. Rubber Chem. Technol. 80, 481–503 (2007)

[18] Lake G.J., Yeoh O.H.: Measurement of rubber ecutting resistance in the absence of friction. Int. J. Fract. 14, 509–526 (1978)

[19] Mars, W.V.: Instrument for measuring the intrinsic strength of polymeric materials via cutting. No.: US 2017/0003207 A1, USA (2017)

[20] Stocek, R., Kratina, O., Kipscholl, R.: A new experimental approach to rubber resistance against cutting by sharp objects. In: Constitutive Models for Rubber IX. Proc. of the 9th European Conference on Constitutive Models for Rubbers, ECCMR 2015, pp. 357–362 (2015)

[21] Reincke, K., Grellmann, W., Kluppel, M.: Investigation of fracture mechanical properties of filler-reinforced styrene-butadiene elastomers. Kautsch. Gummi Kunstst. 5, 246–251 (2009)

[22] Kim, J.H., Jeong, H.Y.: A study on the material properties and fatigue life of natural rubber with different carbon blacks. Int. J. Fatigue 27, 263–272 (2005)

[23] Lake, G.J.: Fatigue and fracture of elastomers. Rubber Chem. Technol. 68, 435–460 (1995)

[24] Ghosh, P., Stocek, R., Gehde, M., *et al.*: Investigation of fatigue crack growth characteristics of NR/BR blend based tyre tread compounds. Int. J. Fatigue 188, 9–21 (2014)

[25] Ghosh, P., Mukhopadhyay, R., Stocek, R.: Durability prediction of NR/BR and NR/SBR blend tread compounds using tear fatigue analyser. Kautsch. Gummi Kunstst. 69, 53–55 (2016)

[26] Eisele, U., Kelbch, S.A., Engels, H.W.: The tear analyzer – A new tool for quantitative measurements of the dynamic crack growth of elastomers. Kautsch. Gummi Kunstst. 45, 1064–1069 (1992)

[27] Stocek, R., Heinrich, G., Gehde, M., *et al.*: Analysis of dynamic crack propagation in elastomers by simultaneous tensile- and pure-shear-mode testing. In: Grellmann, W., *et al*. (eds.) Fracture Mechanics and Statistical Mechanics, pp. 269–301, Springer-Verlag, Berlin Heidelberg (2013)

[28] Stocek, R., Horst, T., Reincke, K.: Tearing energy as fracture mechanical quantity for elastomers. In: Stöckelhuber, K.W., *et al.* (eds.) Designing of Elastomer Nanocomposites: From Theory to Applications. Advances in Polymer Science, pp. 361–398, Springer, New York (2017)

[29] Thomas, A.G.: Rupture of rubber II. The strain concentration at an incision. J. Polym. Sci. 18, 177–188 (1955)

[30] Greensmith, H.W., Thomas, A.G.: Rupture of rubber III. Determination of tear properties. J. Polym. Sci. 18, 189–200 (1955)

[31] Thomas, A.G.: The development of fracture mechanics for elastomers. Rubber Chem. Technol. 67, G50–G60 (1994)

[32] Gent, A.N., Henry, A.W.: On the tear strength of rubbers. In: Proc. of International Rubber Conference, Brighton, pp. 193–204 (1967)

[33] Reincke, K.: Elastomere Werkstoffe – Zusammenhang zwischen Mischungsrezeptur, Struktur und mechanischen Eigenschaften sowie dem Deformations- und Bruchverhalten, Shaker Verlag, (2016)

[34] Grellmann, W., Reincke, K.: Technical material diagnostics – Fracture mechanics of filled elastomer blends. In: Grellmann, W., *et al.* (eds.) Fracture Mechanics and Statistical Mechanics, pp. 227–268, Springer-Verlag, Berlin Heidelberg (2013)

[35] Gent, A.N., Mars, W.V.: Strength of elastomers (Chapter 10). In: Mark, J.E, *et al.* (eds.) The Science and Technology of Rubber (4th Ed.), pp. 473–516, Academic Press, Boston (2013)

[36] Stocek, R., Mars, W.V., Kratina, O., *et al.*: Characterization of ageing effect on the intrinsic strength of NR, BR and NR/BR blends. In: Constitutive Models for Rubber X. Proc. of the 10th European Conference on Constitutive Models for Rubber, ECCMR X 2017, pp. 371–374 (2017)

LIST OF ABBREVIATIONS AND PARAMETERS

CB ..... carbon black

CCD ..... charge-coupled device

BR ..... butadiene rubber

E-SBR ..... emulsion styrene-butadiene-rubber

FCG ..... fatigue crack growth

NR ..... natural rubber

ISA ..... intrinsic strength analyser

ISO ..... international organization for standardization

LLC ..... limited liability company

phr ..... parts per hundred rubber

rpm ..... rotation per minute

SBR ..... styrene-butadiene-rubber

TFA ..... tear and fatigue analyser

USA ..... United States of America

a	[mm]	crack length
B	[mm]	thickness
b	[-]	proportionality constant
β	[-]	material constant
da/dn	[mm/cycle]	fatigue crack growth rate
f	[N]	cutting force
F_C	[J/m^2]	cutting energy
l	[mm]	clamp distance
L_0	[mm]	length of sample
m	[-]	material constant
n	[cycle]	loading cycles
$S_{0,C}$	[J/m^2]	intrinsic cutting energy
T	[J/m^2]	tearing energy
T_0	[J/m^2]	intrinsic strength

T_C [J/m^2]..... ultimate tear strength

W [J]..... recoverable elastic strain energy

W_{dis} [J]..... dissipated energy

W_{ext} [J]..... external work

W_P [mm]..... width of sample

W_{sep} [J]..... local work of separation

LIST OF FIGURE CAPTIONS

Fig. 1. Visualization showing the typical deformation of a crack tip and association of ruptured and not ruptured chains at the vicinity of the crack tip.

Fig. 2. Paris-Erdogan plot showing typical FCG rate, d*a*/d*n* behaviour of rubber in double-logarithmic plot *vs.* energy release rate, *T*.

Fig. 3. The scheme of pure-shear testing specimen.

Fig. 4. The photograph of ISA (left) and the detail on the cut test specimen during operating (right).

Fig. 5. Measurement principle of the ISA, where: A – actuator of the axis Y; B – actuator of the axis X; C – loading cell of the axis X; D – loading cell of the axis Y; E – razor blade; F – test specimen; G – top clamping system of test specimen; H – bottom clamping system of test specimen, I – razor blade tip.

Fig. 6. Method used to determine the intrinsic cutting energy, $S_{0,c}$ from cutting energy, F_c *vs.* tearing energy, T data.

Fig. 7. The photo of TFA (left) and the detail of the isolated chamber (right).

Fig. 8. The results from ISA for NR and BR compound.

Fig. 9. The results from ISA for SBR_{ref} compound.

Fig. 10. Displacement, *l vs*. tearing energy, *T* under fatigue conditions for NR and BR compound.

Fig. 11: FCG rate, d*a*/d*n* as a function of tearing energy, *T* for NR and BR compound.

Fig. 12. Strain, ε as a function of tearing energy, *T* for NR and BR compound.

Fig. 13. Reconstructed complete curve of FCG rate, da/dn as a function of tearing energy, T for NR and BR compound.

LIST OF TABLE CAPTIONS

Figure 1

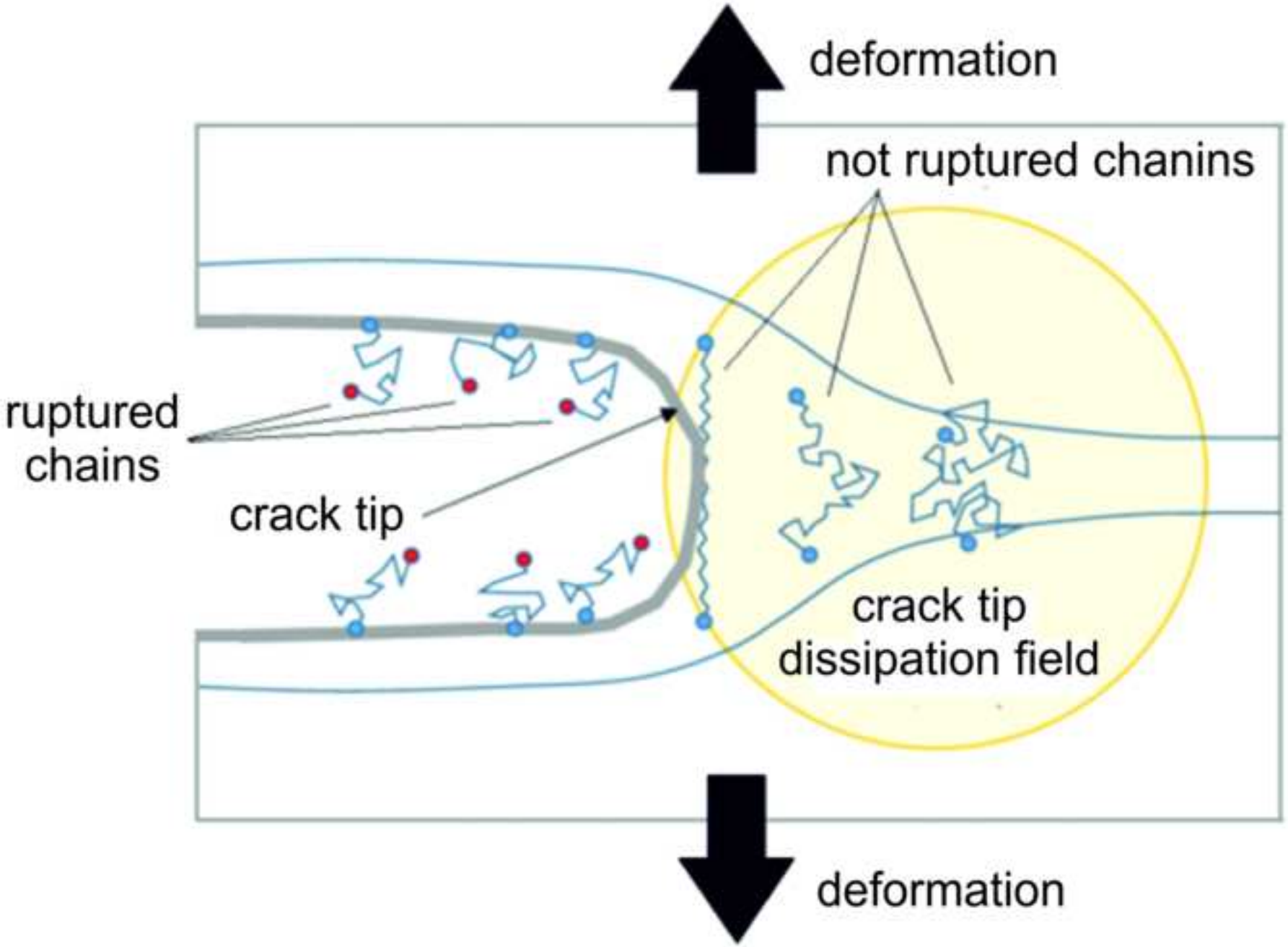

Figure 2

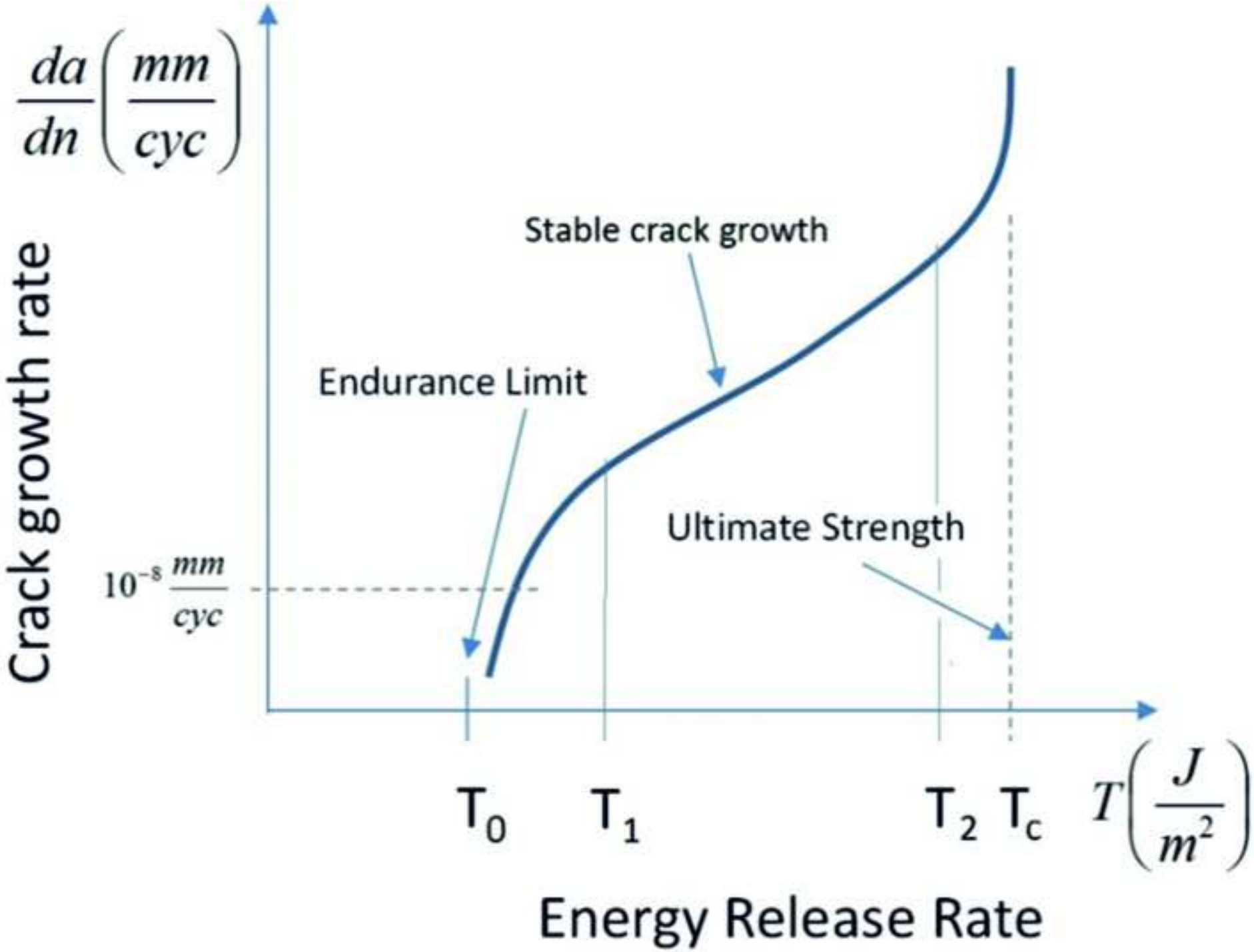

Figure 3

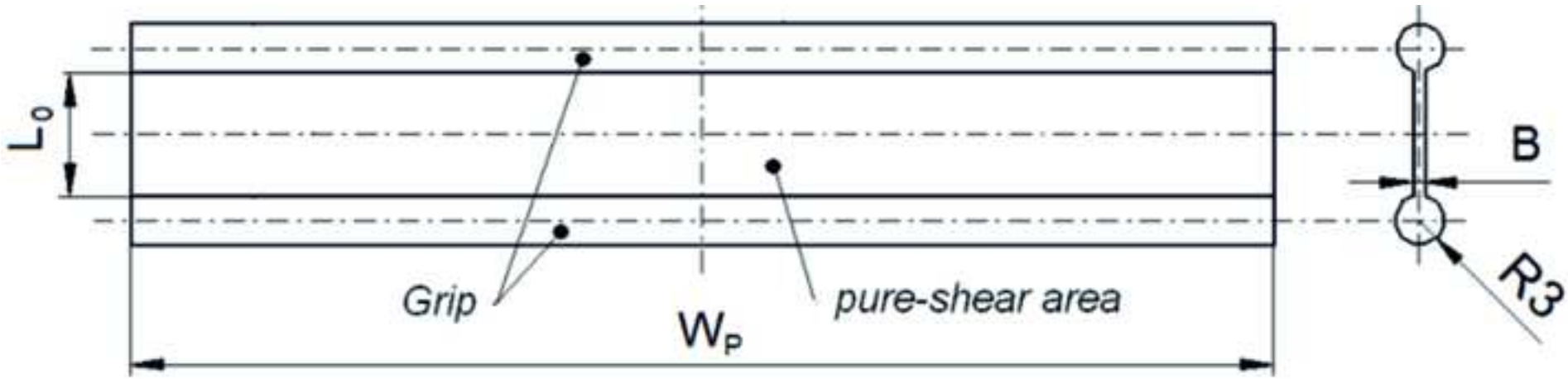

Figure 4

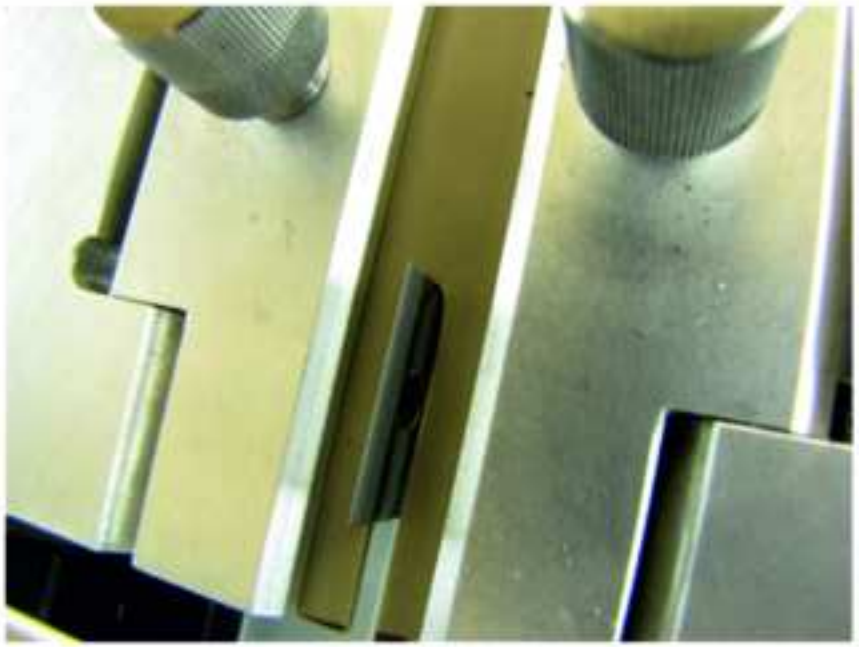

Figure 5

Click here to access/download;Figure;Figure 5_SS7_ID-VIP024_Stocek.tif

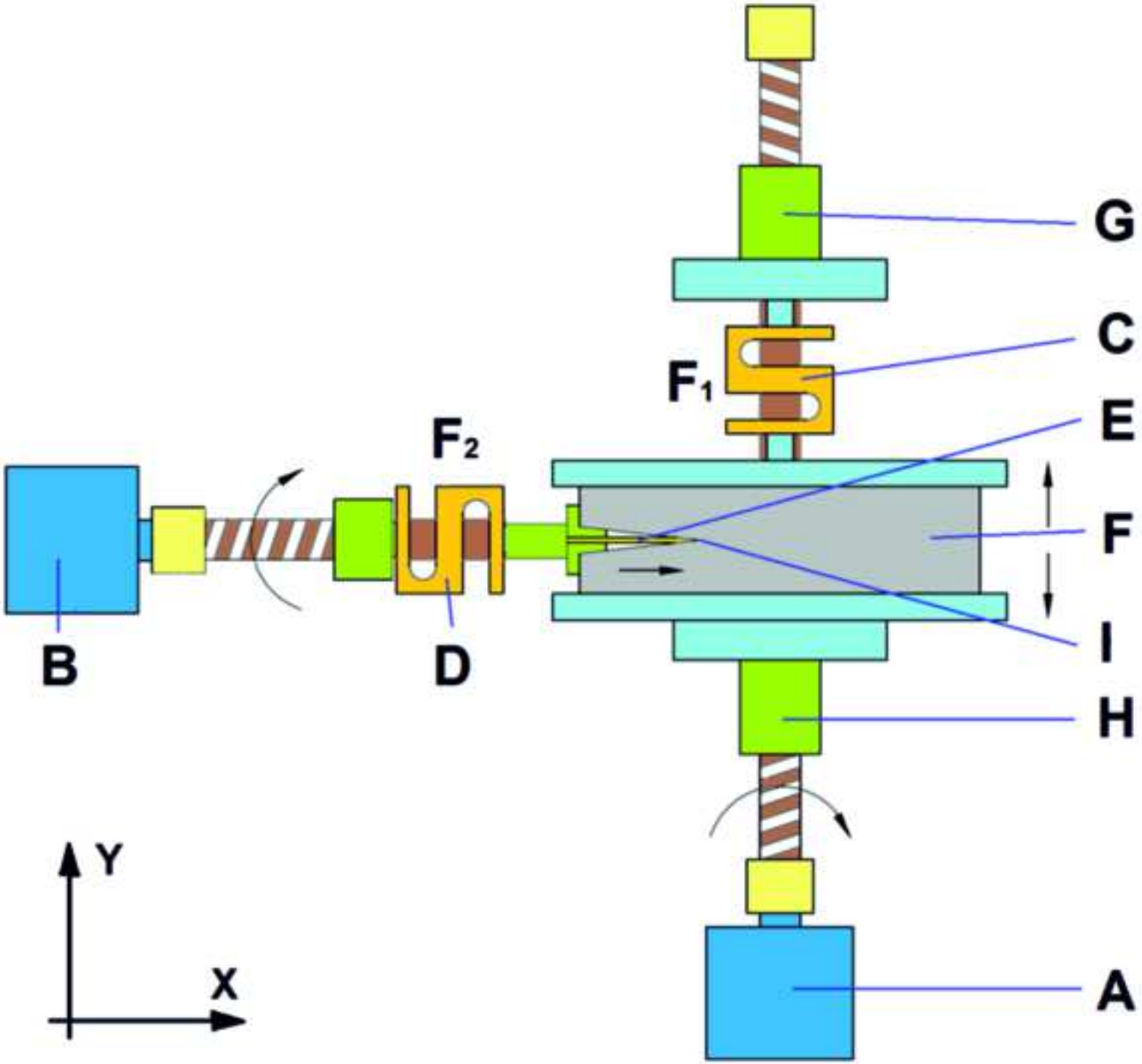

Figure 6

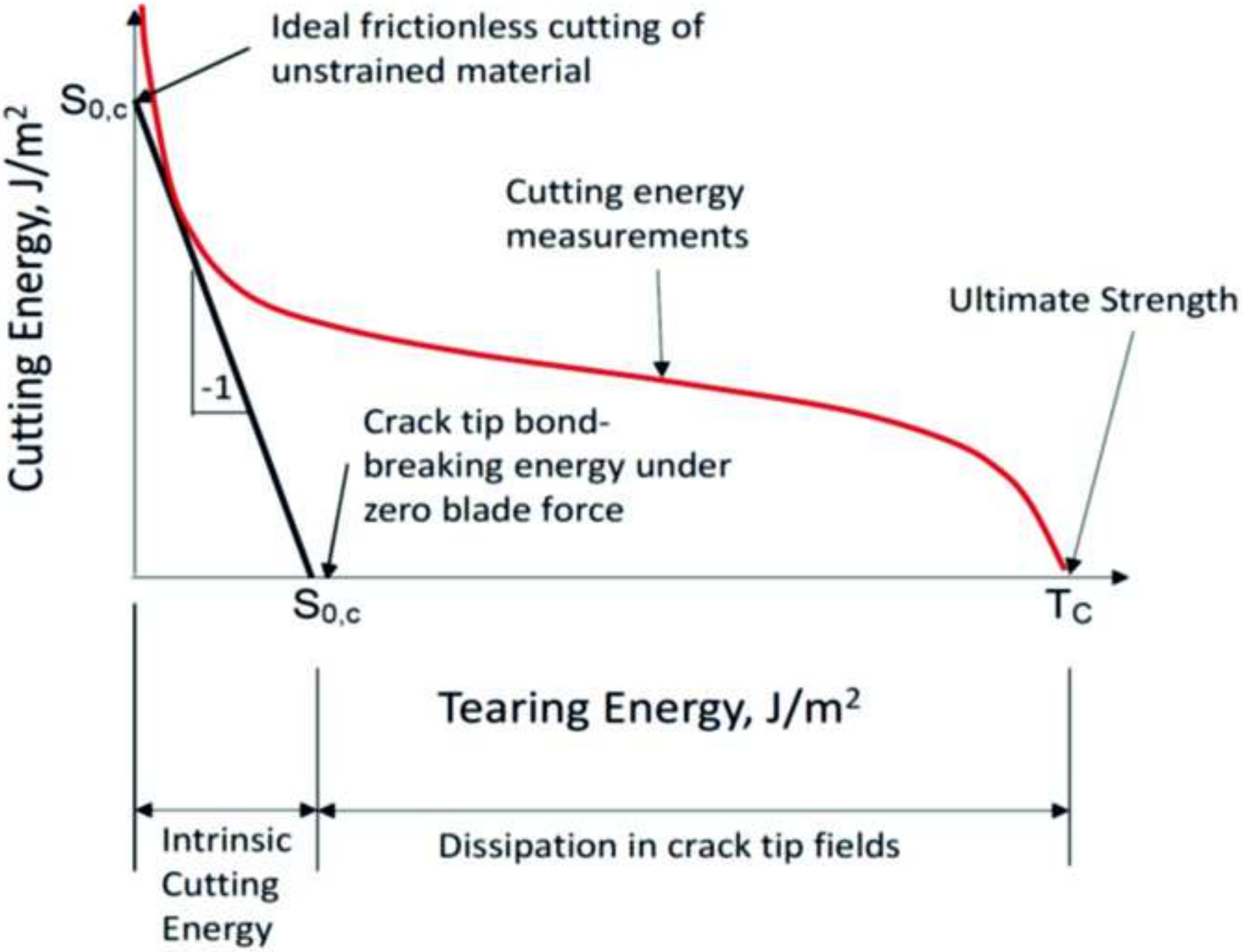

Figure 7

Click here to access/download;Figure;Figure 7_SS7_ID-VIP024_Stocek.tif

Figure 8

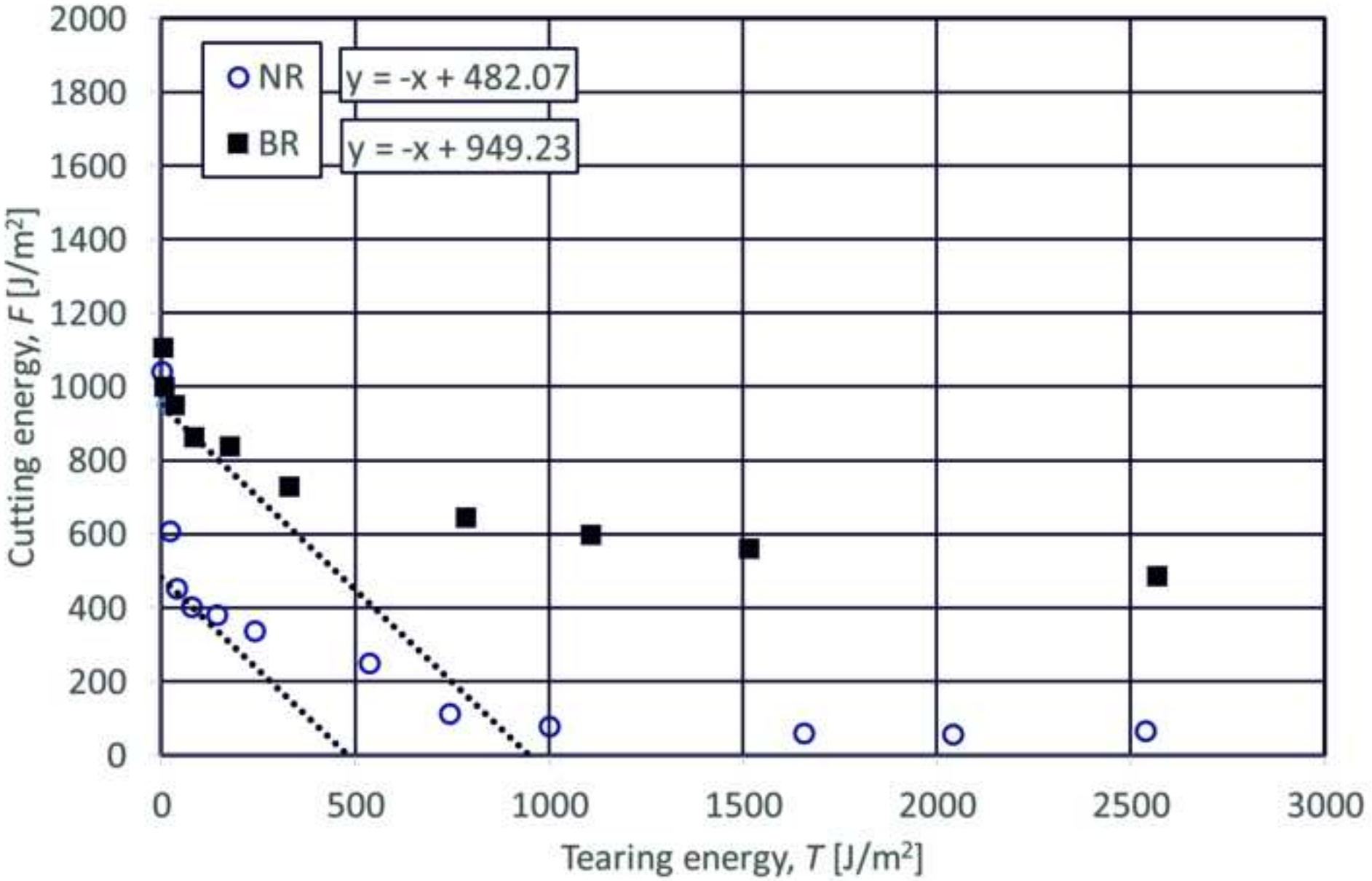

Figure 9

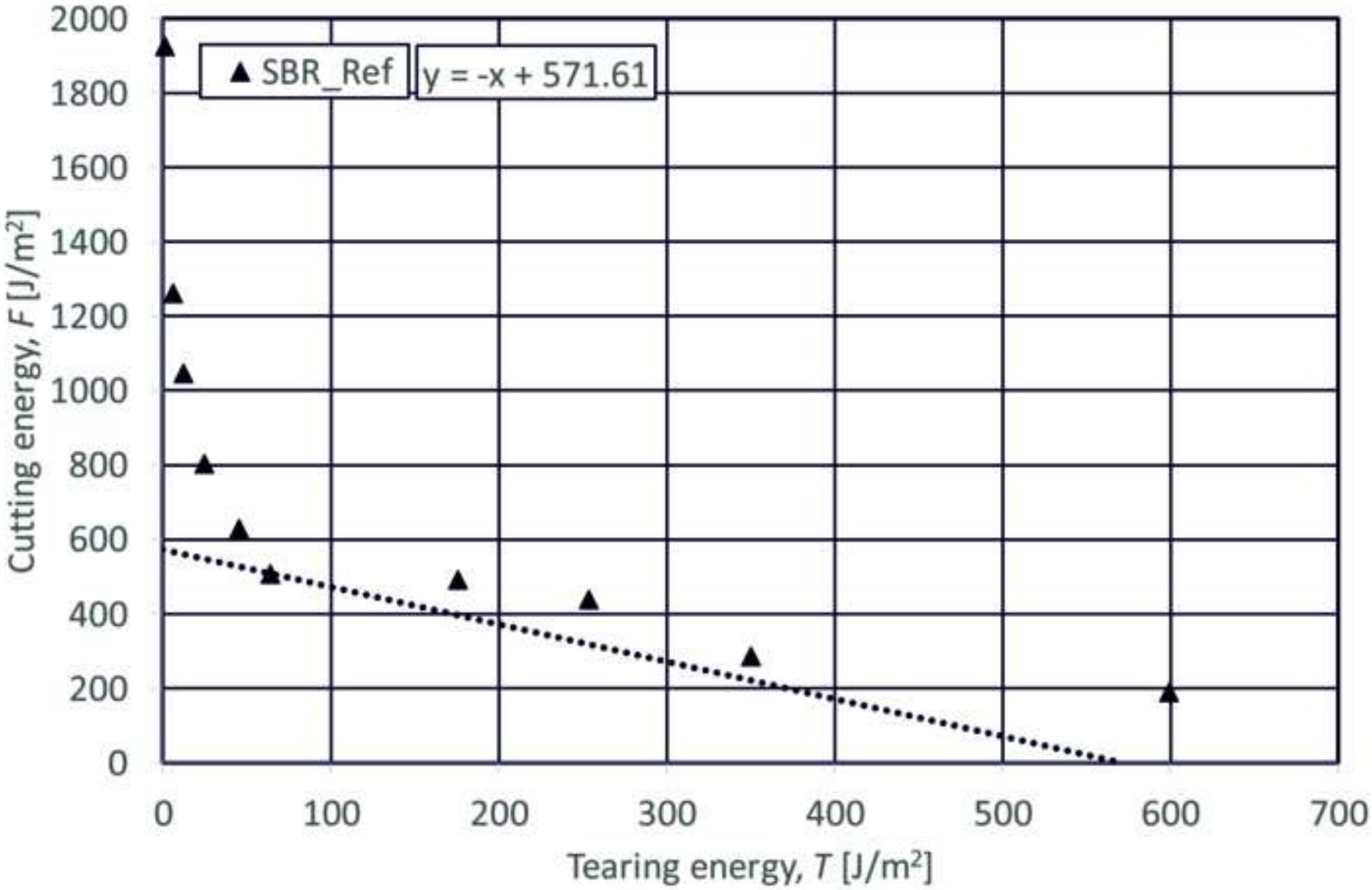

Figure 10

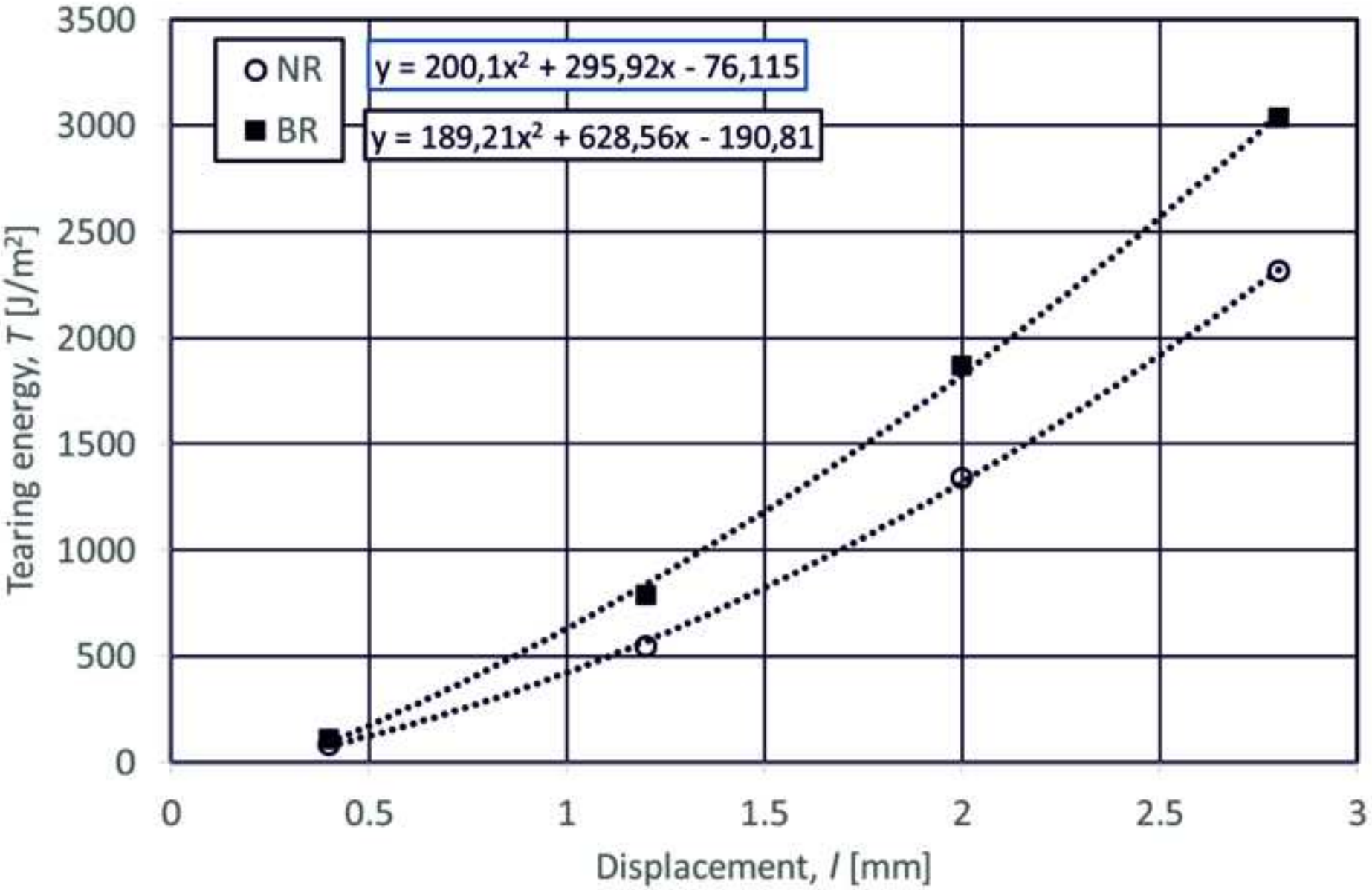

Figure 11

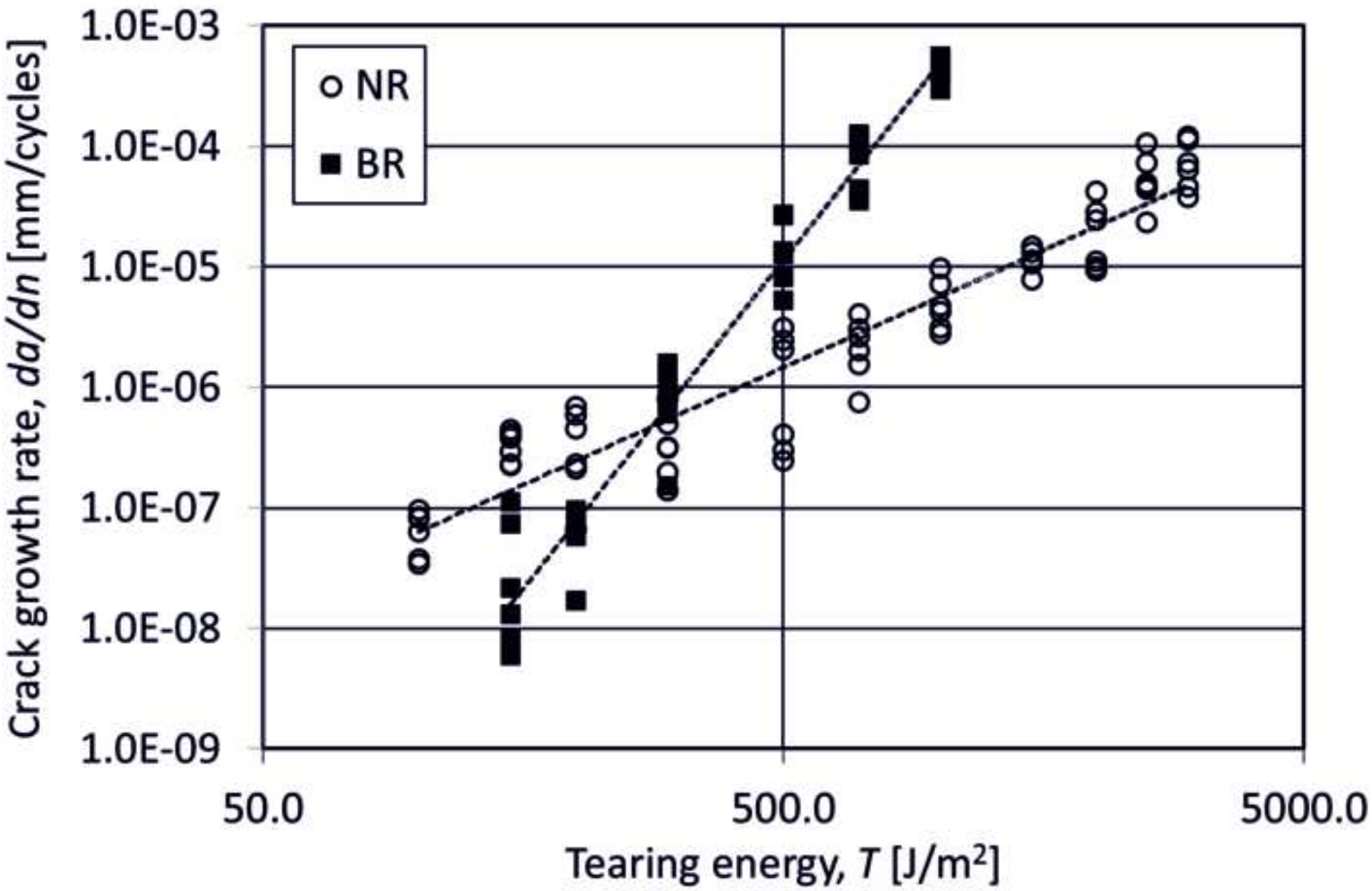

Figure 12

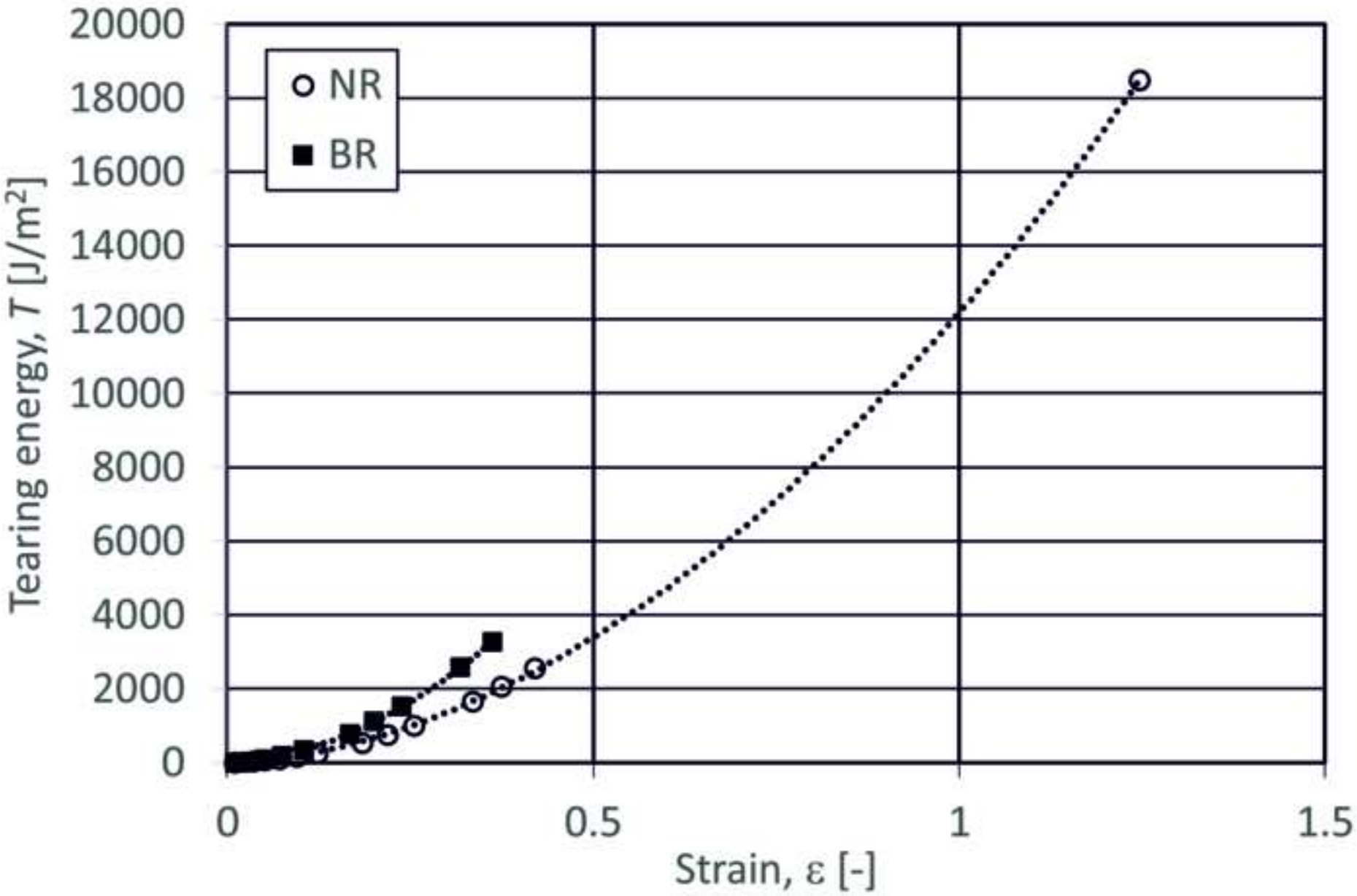

Figure 13

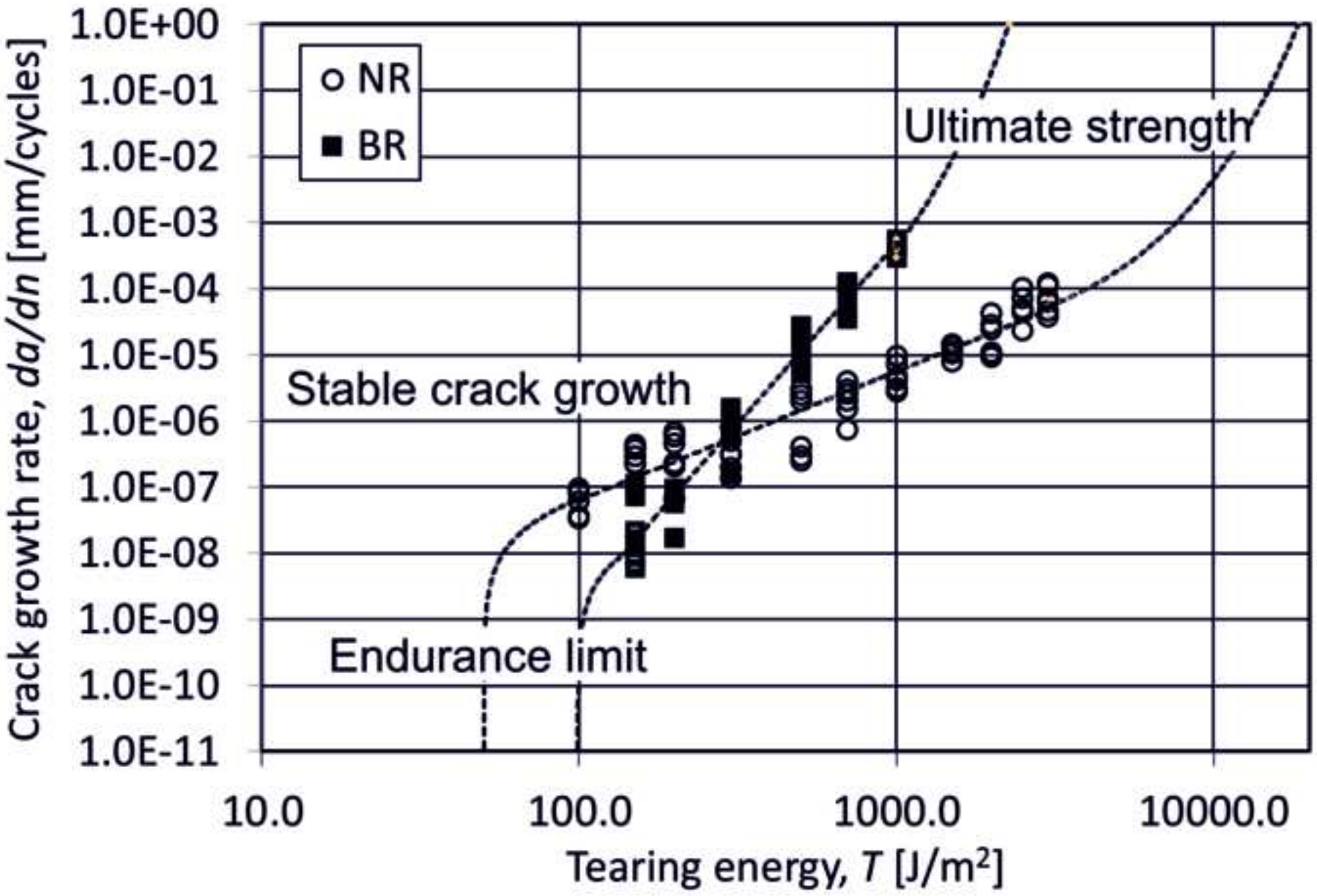

TABLE 1

Formula	**NR**	**BR**
SMR20 NR	100	–
High-Cis Nd-BR	–	100
N339 CB in Master Batch	50	50
Zinc oxide	2	2
Stearic acid	1	1
Sulphur	2	2
TBBS[a)]	1	2
MTBS[b)]	–	0.5
6PPD[c)]	1	1
Total (phr):	157	158.5

a) N-tert-butyl-benzothiazole sulfonamide
b) Benzothiazole disulfide
c) N-(1,3-Dimethylbutyl)-N´-phenyl-1,4-benzenediamine

TABLE 2

Formula	**SBR_{ref}**
E-SBR 1500	100
Zinc oxide	5
Stearic acid	2
Sulphur	1.75
CBS[a)]	1
6PPD[b)]	1
Total phr:	110.75

a) N-cyklohexyl-2-benzthiazole sulfenamide
b) N-(1,3-Dimethylbutyl)-N´-phenyl-1,4-benzenediamine

Table 3

TABLE 3

Loading mode	**Pulse-width frequency, f_1 [Hz]**	**Loading frequency, f_2 [Hz]**	**Temperature, T_e [°C]**	**Pre-force, F_{pre} [N]**
Gaussian pulse	10	5	28	1

Table 4

TABLE 4

Sample	Stress @100 % elongation [MPa]	Stress @300 % elongation [MPa]	Stress @break [MPa]	Strain @break [%]
NR	2.0±0.2	8.9±0.8	22.9±3.1	599±63
BR	2.9±0.1	9.6±0.4	9.8±0.9	284±20

Table 5

TABLE 5

Sample	Shore-A hardness [ShA]	Abrasion volume loss [mm^3]
NR	57.0±0.7	174.9±4.8
BR	68.2±0.4	52.0±0.9

TABLE 6

Sample	Intrinsic cutting energy, $S_{0,c}$ [J/m^2]	Proportionality constant, b [-]	Intrinsic strength, T_0 [J/m^2]
NR	482.07	0.105	50.62
BR	949.23		99.67

TABLE 7

Sample	FCG, d*a*/d*n* [mm/cyc]	Material parameter, β [mm]	Material parameter, *m* [-]
NR	$\beta . T^m$	8.10^{-12}	1.9448
BR	$\beta . T^m$	2.10^{-20}	5.4464